

A reduced-order framework for three-dimensional-equivalent confined groundwater modeling with emphasis on well-boundary implementation

Saumava Dey¹  · Anirban Dhar¹

Received: 12 August 2022 / Accepted: 29 June 2023 / Published online: 31 July 2023
© The Author(s), under exclusive licence to International Association of Hydrogeologists 2023

Abstract

Groundwater management frameworks rely on budget-friendly mathematical groundwater flow models for identifying sustainable policies. Such models should be capable of modeling well-flow hydraulics and aquifer dynamics simultaneously. A robust well-flow model considers the finite well radius to estimate the hydraulic head distribution in and around a pumping well, considering the effects of partial well penetration, well-bore storage, and well-bore skin. This paper introduces the concept of well-boundary to develop a three-dimensional (3D)-equivalent 2D confined groundwater flow modeling framework for monitoring natural aquifer systems. The developed OpenFOAM®-based model—*modFlowFOAM*—implements the analytical solution of the well-hydraulics problem for confined aquifer systems as a Dirichlet boundary condition on the well boundary to account for the vertical flow in the neighborhood of the pumping well. To minimize the computational burden (CPU time and usage) involved in modeling large-scale confined aquifer systems, a reduced-order modeling solver for the *modFlowFOAM* library has also been developed. The numerical results of *modFlowFOAM* depict excellent correspondence with the MODFLOW results and other numerical results presented in the literature for various well-hydraulics and confined-aquifer flow problems involving regional and synthetic aquifer systems. The accuracy and efficiency of *modFlowFOAM* ensure its potential applicability to characterize the dynamics of confined aquifer systems.

Keywords Well-boundary · Pumping/well test · Groundwater flow · Reduced-order model · OpenFOAM®

Introduction

Well-flow problems in confined and unconfined aquifers are important to the study of subsurface hydrology. Numerical modeling of well hydraulics in porous media is essential for the continuous assessment of groundwater dynamics and parameter characterization of natural aquifer systems. Well-flow characteristics are different in confined and unconfined aquifer systems depending on the mechanism of water release from storage. Impermeable surfaces bound a confined aquifer on the upper and lower boundaries, restricting

the vertical inflow and outflow processes to and from the aquifer. In response to extraction through pumping wells, water is released from storage due to compression of the aquifer matrix and subsequent expansion of water. When a pumping well completely penetrates the thickness of the confined aquifer, the flow toward the well is horizontal. On the other hand, in a partially penetrating pumping well, both horizontal and vertical flow components are dominant as the flowlines converge while approaching the well-screen. A generalized numerical framework for well-flow modeling should consider the anisotropy of the porous media alongside the effects of finite well radius, well-bore storage, well-bore skin, and the extent of penetration of the pumping well into the aquifer, in order to estimate the drawdown within the pumping well and in its neighborhood (Yeh and Chang 2013). Regional-scale modeling of confined aquifer systems does not usually require simulation of vertical flow except for highly heterogeneous or karstic aquifers where three-dimensional (3D) flow is significant. Two-dimensional (2D) groundwater flow modeling is performed as confined aquifer

✉ Saumava Dey
dey.saumava@gmail.com

Anirban Dhar
anirban@civil.iitkgp.ac.in

¹ Civil Engineering Department, Indian Institute of Technology Kharagpur, Kharagpur, West Bengal 721302, India

flow is mostly horizontal except in the locality of the pumping wells in the case of partial penetration. Moreover, for monitoring confined aquifer systems, point measurements of hydraulic heads are recorded over the horizontal stretch of the aquifer domain. Large-scale modeling of aquifer dynamics and well hydraulics for natural confined aquifer systems requires the development of accurate and computationally inexpensive numerical models. Hence, the focus should be on developing a 3D equivalent modeling framework for 2D confined groundwater flow (accounting for the vertical flow in the neighborhood of the pumping well) without solving the 3D governing equations. To model the effects of vertical flow utilizing a 2D numerical framework, a suitable analytical solution for the well-hydraulics problem needs to be incorporated into the modeling framework.

Theis (1935) was the first to formulate an analytical solution for transient water flow into a fully penetrating pumping well of minimal diameter in a homogeneous and isotropic nonleaky confined aquifer of infinite areal extent and uniform thickness. Since then, many analytical models have been developed to represent realistic field conditions in confined aquifers. Barenblatt et al. (1960) conducted studies on unsteady seepage in fissured rocks and presented analytical solutions assuming complete penetration of the pumping well. The effect of partial penetration of pumping wells and anisotropy of confined aquifer systems on well hydraulics was first introduced by Hantush (1961). Agarwal et al. (1970) presented analytical solutions for transient confined aquifer flow considering well-bore storage and skin effects for fully penetrating pumping wells. A modified solution of the well-hydraulics problem for heterogeneous aquifer formations was presented by Streltsova-Adams (1978). However, the leading-edge analytical model for well-hydraulics problems for confined double-porosity aquifers was presented by Dougherty and Babu (1984), including the effects of well-bore storage and skin for unsteady flow into a fully or partially penetrating pumping well of finite diameter. Consequently, several analytical solutions have been developed for well-flow modeling in confined aquifer systems under varying practical considerations (Zhan and Park 2003; Yeh et al. 2008; Barua and Bora 2010; Wen et al. 2017; Fan and Parashar 2020).

Several numerical methods have been applied for estimating groundwater dynamics in natural aquifer systems. The finite difference (FD) based computer model MODFLOW (Harbaugh 2005) has wide application in groundwater modeling of unconfined and confined aquifer systems. MODFLOW-USG (Panday et al. 2013), the control volume finite-difference (CVFD) based unstructured grid version of MODFLOW, was developed to solve complex-geometry groundwater flow problems. MODFLOW-USG uses the WEL package for simulating steady flow into pumping wells. The finite volume (FV) based confined groundwater

flow model developed by Dey and Dhar (2020) claims better grid-convergence than MODFLOW in estimating well drawdown for quasi-steady flow problems subjected to point source singularity; however, its applicability is limited to problems related to steady flow through fully penetrating pumping wells. Presently, the revised Multi-Node Well (MNW2) package for MODFLOW (Konikow et al. 2009) has been developed for more realistic and reliable modeling of regional aquifer systems allowing drawdown corrections for the effects of partial penetration and well-bore storage. The FV method is inherently mass-conservative and suitable for domains with complex geometries as it can be applied to irregular unstructured grid systems. OpenFOAM® (Jasak et al. 2007) is a universally accepted open-source FV-based computational fluid dynamics toolbox that facilitates parallel computation through domain decomposition. OpenFOAM® has been utilized in subsurface hydrology for modeling variably saturated flow in porous media. Several OpenFOAM®-based saturated-unsaturated flow models are available in the literature, e.g., *suGWFOam* (Liu 2013), *RichardsFOAM* (Orgogozo et al. 2014; Orgogozo 2015, 2022), *porousMultiphaseFoam* (Horgue et al. 2015), and *subsurfaceFlowFOAM* (Dey and Dhar 2022).

The accuracy of a numerical model highly depends on the discretization of the spatial and temporal domains. With the refinement of the grid system, the accuracy of the model predictions is improved, which increases computational expense, making it inefficient in the case of large-scale models. Over the past few decades, the concept of reduced-order modeling has emerged in different scientific studies (Sirovich 1987; Park and Cho 1996; Park et al. 1999; Haasdonk and Ohlberger 2011; Hasenauer et al. 2012). Reduced-order modeling scales down the original problem, thereby requiring a significantly lesser number of algebraic equations to be solved per time iteration. The model order reduction methodology has also been extended to groundwater flow and transport modeling. The techniques of model order reduction applied to groundwater studies can be roughly categorized as data-driven, projection-based, and structural reduction methods. However, the application is restricted to only saturated flow modeling through confined and unconfined aquifer systems with no attempt toward variably saturated subsurface flow modeling in the literature. Low-dimensional groundwater flow models have been developed for homogeneous or uniformly distributed heterogeneous confined (Vermeulen et al. 2004; Pasetto et al. 2011, 2013; Boyce and Yeh 2014; Dey and Dhar 2020) and unconfined (Boyce et al. 2015; Stanko et al. 2016) aquifer systems. The reduced-order groundwater flow models have added a new dimension to computational hydrology, whereby they significantly cut down the computational expenses in CPU time and usage otherwise incurred in simulating the groundwater dynamics for

regional-scale aquifer systems involving complex geometries over large time scales.

This paper presents a generalized 2D FV-based full-system mathematical model (*confinedGWFlowFOAM*) and a corresponding reduced-order model (*reducedConfinedGWFlowFOAM*) for simulating the hydrodynamics of confined aquifer systems considering the effects of the vertical flow components around the pumping well arising from partial well penetration and anisotropy of the porous media. The novelty of the present work lies in the concept of *well-boundary*—a boundary condition proposed for modeling both steady and unsteady flow into fully or partially penetrating pumping wells accounting for the effects of finite well radius, well-bore storage, well-bore skin, and partial penetration. The models have been developed utilizing the OpenFOAM® framework, which is a unique attempt to develop a computationally inexpensive and efficient open-source mathematical framework for confined groundwater flow modeling.

Development of *modFlowFOAM*

modFlowFOAM is a confined groundwater flow model developed using the OpenFOAM® framework. *modFlowFOAM* constitutes two solvers: *confinedGWFlowFOAM*, a full-system model for evaluating the hydraulic head distribution in a confined aquifer system, and *reducedConfinedGWFlowFOAM*, a Galerkin Projection based reduced-order confined groundwater flow model.

confinedGWFlowFOAM

The *confinedGWFlowFOAM* solver has been developed based on the continuity equation governing the transient flow of saturated groundwater through a heterogeneous and anisotropic confined aquifer subjected to pumping, which can be expressed as follows (Bear 1979):

$$S_s \frac{\partial z_a(\underline{x}, t)}{\partial t} - \nabla \cdot \left[\underline{\underline{K}} \nabla z_a(\underline{x}, t) \right] + W_s + \sum_{i=1}^{n_p} N_s(\underline{x}, t) \delta(\underline{x} - \underline{x}_i, t) = 0 \quad (1)$$

$$\underline{x} \in \Omega \quad t \in [0, T_{\text{final}}]$$

where z_a is the hydraulic head [L], \underline{x} is the vector of space coordinates in Euclidean space [L], t is the time coordinate [T], $\underline{\underline{K}}$ is the hydraulic conductivity tensor [LT^{-1}], S_s is the specific storage [L^{-1}], W_s is the specific volumetric source/sink [T^{-1}], N_s is the specific volumetric point source/sink [T^{-1}], n_p is the number of operative pumping wells, T_{final} is the final simulation time [T], δ is the Dirac delta function, and Ω represents the physical domain. The hydraulic

conductivity tensor can be represented as $\underline{\underline{K}} = \begin{bmatrix} K_x & 0 \\ 0 & K_y \end{bmatrix}$, where K_x and K_y are the hydraulic conductivities in the X and Y directions, respectively [LT^{-1}].

The pumping well has been considered to be completely penetrating for ensuring horizontal flow unless mentioned otherwise. A constant pumping rate has been assumed for the pumping well throughout the time domain. Depth-averaged hydraulic head has been defined in the governing Eq. (1) to describe the horizontal movement of groundwater, thereby reducing the flow in 2D space. The governing equation is subjected to the following initial and boundary conditions:

Initial condition

$$z_a(\underline{x}, 0) = z_{a0}(\underline{x}) \quad (2)$$

where z_{a0} is the known function of hydraulic head at initial time [L].

Dirichlet boundary condition

$$z_a(\underline{x}, t) = z_{aD}(\underline{x}, t) \quad \underline{x} \in \Gamma_D \subset \partial\Omega \quad (3)$$

where z_{aD} is the known function of hydraulic head on the Dirichlet boundary [L] and Γ_D represents the Dirichlet boundary.

Neumann boundary condition

$$-\underline{\underline{K}} \nabla z_a(\underline{x}, t) \cdot \hat{\underline{n}} = q_N(\underline{x}, t) \quad \underline{x} \in \Gamma_N \subset \partial\Omega \quad (4)$$

where q_N is the known flux function [LT^{-1}], $\hat{\underline{n}}$ is the normal unit vector at the boundary, and Γ_N represents the Neumann boundary.

Well-boundary condition

Unsteady flow into fully or partially penetrating wells must be considered for more realistic modeling of well-flow problems in confined aquifer systems. The effects of partial penetration combined with the anisotropy of the porous media cause vertical flow to predominate in the vicinity of the pumping well. Thus, the governing Eq. (1) is not valid in the neighborhood of the pumping well and is only applicable where the flow becomes horizontal. This paper introduces the concept of *well-boundary*—a circular boundary at a radial distance r from the center of the pumping well where the vertical flow component vanishes and the flow becomes horizontal. In the case of fully penetrating

pumping wells, the flow is horizontal; therefore, the well-boundary can be considered at any suitable distance away from the pumping well. However, for partially penetrating wells, the vertical flow gradients become negligible at a radial distance r calculated from the following criterion (Hantush 1961, 1964):

$$r > \frac{1.5b}{\sqrt{\frac{K_z}{K_r}}} \quad (5)$$

where b is the thickness of the confined aquifer [L], and K_r and K_z are the hydraulic conductivities in the radial and vertical directions from the center of the pumping well [LT^{-1}]. Hence, the location of the well-boundary from the center of the pumping well is estimated from Eq. (5) for modeling the flow dynamics in a confined aquifer arising from partially penetrating wells.

One of the significant challenges in the numerical modeling of well-flow problems in natural aquifer systems is specifying the finite radius of the pumping well (r_w). For steady flow into pumping wells, the well-boundary is a Neumann boundary assumed to be located at the radial distance r_w from the center of the pumping well. On the other hand, for unsteady flow into pumping wells, the well-boundary is a time-varying Dirichlet boundary where there is a numerically inverted Laplace domain analytical solution of dimensionless drawdown for flow to a fully or partially penetrating well of finite diameter in confined aquifers (Dougherty and Babu 1984), considering the effects of vertical flow have been implemented. The hydraulic head on the well-boundary at every time step can be expressed as follows:

$$z_{ao}(\mathbf{x}, t) = z_{a0}(\mathbf{x}) - s_{ao}(\mathbf{x}, t) \quad (6)$$

where z_{ao} and s_{ao} are the hydraulic head and drawdown at the well-boundary, respectively [L].

The Laplace transform of the dimensionless drawdown within the pumping well (\bar{s}_{awD}) and at the well-boundary (\bar{s}_{aoD}) at a radial distance r from the center of the pumping well can be expressed as follows:

$$\bar{s}_{awD}(p_c) = \frac{2(A_c + A_0 + S_w)}{p_c(l_D - d_D)[1 + W_D p_c(A_c + A_0 + S_w)]} \quad (7)$$

$$\bar{s}_{aoD}(r_D, p_c) = \frac{2(E_c + E_0)}{p_c(l_D - d_D)[1 + W_D p_c(A_c + A_0 + S_w)]} \quad (8)$$

where

$$A_0 = \frac{K_0(q_{10})(l_D - d_D)}{q_{10}K_1(q_{10})} \quad (9)$$

$$E_0 = \frac{K_0(q_{20})(l_D - d_D)}{q_{10}K_1(q_{10})} \quad (10)$$

$$A_c = \frac{2}{(l_D - d_D)} \sum_{n=1}^{\infty} \frac{K_0(q_{1n}) \{ \sin[n\pi(1-d_D)] - \sin[n\pi(1-l_D)] \}^2}{n^2 \pi^2 q_{1n} K_1(q_{1n})} \quad (11)$$

$$E_c = 2 \sum_{n=1}^{\infty} \frac{K_0(q_{2n}) \cos(n\pi z_D) \{ \sin[n\pi(1-d_D)] - \sin[n\pi(1-l_D)] \}}{n\pi q_{1n} K_1(q_{1n})} \quad (12)$$

$$q_{10} = \sqrt{p_c} \quad (13)$$

$$q_{20} = q_{10} r_D \quad (14)$$

$$q_{1n} = (p_c + n^2 \pi^2 \beta_{cD})^{0.5} \quad (15)$$

$$q_{2n} = q_{1n} r_D \quad (16)$$

where K_0 and K_1 are the zero-order and first-order modified Bessel functions of the second kind, respectively.

The summations in Eqs. (11) and (12) are computed for \bar{N}_c terms, where \bar{N}_c can be evaluated as follows:

$$\bar{N}_c = \max \left\{ \bar{N}_{c\min}, \min \left\{ \bar{N}_{c\max}, \bar{N}_{c\max} 2^{[-\log_{10}(\beta_c)-2]} \right\} \right\} \quad (17)$$

For all the test examples, the values of $\bar{N}_{c\min}$ and $\bar{N}_{c\max}$ have been assumed as 4 and 30, respectively. The numerical inversion of the Laplace domain solutions has been performed by applying the Stehfest algorithm (Stehfest 1970) to evaluate the dimensionless drawdown values \bar{s}_{awD} and \bar{s}_{aoD} . The Stehfest algorithm calculates the dimensionless drawdown s_{awD} and s_{aoD} as follows:

$$s_{awD}(t_D) = \frac{\ln 2}{t_D} \sum_{j=1}^{N_{sf}} W_j \bar{s}_{awD}(p_c) \quad (18)$$

$$s_{aoD}(t_D) = \frac{\ln 2}{t_D} \sum_{j=1}^{N_{sf}} W_j \bar{s}_{aoD}(r_D, p_c) \quad (19)$$

where

$$p_c = j \frac{\ln 2}{t_D} \quad (20)$$

$$W_j = (-1)^{\left(\frac{N_{sf}}{2} + j\right)} \sum_{k=\frac{j+1}{2}}^{\min(j, \frac{N_{sf}}{2})} \frac{k^{\left(\frac{N_{sf}}{2}\right)} 2k!}{\left(\frac{N_{sf}}{2} - k\right)! k! (k-1)! (j-k)! (2k-j)!} \quad (21)$$

where N_{sf} is the number of terms used in the Stehfest algorithm. The expressions for the dimensionless parameters used in the calculation of s_{ao} and s_{aw} are listed in Table 1.

In Table 1, z is the depth below the top confining layer [L], d is the depth of the top of the well-screen below the top confining layer [L], l is the depth of the bottom of the well-screen below the top confining layer [L], d_s is the thickness of the well-bore skin [L], K_{sw} is the hydraulic conductivity of the well-bore skin [LT^{-1}], r_{wc} is the inside radius of the pumping well in the interval where water levels change during pumping [L], s_{aw} is the drawdown within the pumping well [L], and Q_p is the pumping rate [L^3T^{-1}].

The *confinedGWFlowFOAM* solver can solve a wide range of steady and unsteady flow problems. Also, *confinedGWFlowFOAM* is adept at solving point source singularity problems considering the effects of finite well radius, and well-bore storage, skin, and partial penetration.

confinedGWFlowROM

confinedGWFlowROM is an OpenFOAM® library for proper orthogonal decomposition (POD)-based reduced-order modeling of groundwater flow through heterogeneous and anisotropic confined aquifer systems. POD is a numerical technique implemented to reduce the dimensional complexity associated with computationally expensive simulations. Reduced-order modeling is a computationally economical and efficient technique used as an alternative to full-system groundwater flow models. The proposed reduced-order model approximates the hydraulic

Table 1 Dimensionless parameters and expressions involved in drawdown calculation for unsteady flow into a pumping well in a confined aquifer

Dimensionless Parameter	Expression
r_{wD}	$\frac{r_w}{b}$
r_D	$\frac{r}{r_w}$
l_D	$\frac{l}{b}$
d_D	$\frac{d}{b}$
z_D	$\frac{z}{b} = 0.5$
t_D	$\frac{K_r t}{r_w^2 S_s}$
β_{cD}	$\frac{K_z r_{\text{wD}}^2}{K_r}$
β_c	$\beta_{\text{cD}} r_D^2$
S_w	$\frac{K_r d_s}{K_{\text{sw}} r_w}$
W_D	$\frac{r_{\text{wc}}^2}{2r_w^2 S_s (l - d)}$
s_{aoD}	$\frac{4\pi K_r b s_{\text{ao}}}{Q_p}$
s_{awD}	$\frac{4\pi K_r b s_{\text{aw}}}{Q_p}$

head as the product of an orthogonal matrix $\mathbf{P}(\underline{\mathbf{x}})$ and a time-dependent coefficient vector $\mathbf{r}_n(t)$ as follows:

$$\hat{\mathbf{z}}_a(\underline{\mathbf{x}}, t) = \mathbf{P}(\underline{\mathbf{x}}) \mathbf{r}_n(t) \quad (22)$$

where $\hat{\mathbf{z}}_a$ is the hydraulic head vector estimated by the reduced-order model [L], \mathbf{P} is the POD basis matrix, and \mathbf{r}_n is the time-dependent coefficient vector. The procedure of reduced-order modeling is performed in three steps with the help of three separate applications, which are illustrated in the following subsections.

snapshotMatrix

In the first step of reduced-order modeling, a snapshot matrix that stores the solutions of a full-system groundwater model at some predefined times (snapshot time-set) is formed. The aquifer dynamics change rapidly with the onset of pumping operations for confined groundwater flow problems. Hence, the ‘snapshot time-set’ has been selected by the following function:

$$\tilde{t}_{si} = \begin{cases} 0, & i = 1 \\ \tilde{T}_s \left[1 - \tanh \left(\tilde{c} (1 - u_i) \right) \right], & \text{otherwise} \end{cases} \quad (23)$$

where \tilde{t}_s is the snapshot time-set [T], \tilde{T}_s is the final snapshot time [T], and

$$u_i = \frac{i - 1}{\left(n_{\tilde{t}_s} - 1 \right)}$$

where $n_{\tilde{t}_s}$ is the number of snapshots in each snapshot set. Moreover, \tilde{c} is a constant whose value is chosen carefully depending on two factors—the nature of the problem (quasi-steady or unsteady) and the final snapshot time. The dimension of the final snapshot matrix depends on the number of independent pumping wells operating within the aquifer domain. A single set of snapshots is collected separately for each pumping well operating at a constant rate, while the other wells remain inoperative. For an aquifer system with n_{set} active pumping wells, the final snapshot matrix can be represented as follows:

$$\mathbf{S}_{\text{snap}}^j = \left[\mathbf{z}_a|_{\tilde{t}_{s1}}, \mathbf{z}_a|_{\tilde{t}_{s2}}, \mathbf{z}_a|_{\tilde{t}_{s3}}, \dots, \mathbf{z}_a|_{\tilde{t}_{s_{n_{\tilde{t}_s}}}} \right] \quad \forall j = 1, 2, 3, \dots, n_{\text{set}}$$

$$\mathbf{S}_{\text{snap}} = \left[\mathbf{S}_{\text{snap}}^1, \mathbf{S}_{\text{snap}}^2, \mathbf{S}_{\text{snap}}^3, \dots, \mathbf{S}_{\text{snap}}^{n_{\text{set}}} \right] \quad (24)$$

where \mathbf{S}_{snap} is the snapshot matrix.

The *snapshotMatrix* application utilizes the *confinedGWFlowFOAM* solver to compute a set of snapshots at the time instants given by Eq. (23). For multiple pumping wells in the aquifer domain, separate sets of snapshots are captured, which are finally merged to form the final snapshot

matrix \mathbf{S}_{snap} . The input parameters for running the *snapshot-Matrix* application are n_{t_s} , \tilde{c} , and T_s .

preComputation

In the next step, singular value decomposition (SVD) was performed for orthonormalization of the final snapshot matrix \mathbf{S}_{snap} as follows:

$$\mathbf{S}_{\text{snap}} = \mathbf{U}\Sigma\mathbf{V}^T \quad (25)$$

where \mathbf{U} and \mathbf{V} are the matrices of the left and right singular vectors, respectively, and Σ is the diagonal matrix with the singular values as the diagonal elements. In Eq. (25), the matrix \mathbf{U} is the POD basis containing the left singular vectors of \mathbf{S}_{snap} . Among all POD basis vectors, those which exhibit maximum information regarding the system dynamics are chosen based on their corresponding singular values to form the final POD basis \mathbf{P} . The selection criterion can be represented as follows:

$$\frac{\sum_{i=1}^{\tilde{n}_p} \sigma_i}{\sum_{i=1}^{\text{Rank}(\mathbf{S}_{\text{snap}})} \sigma_i} \times 100\% \geq 99.99\% \quad (26)$$

where \tilde{n}_p is the number of principal components and σ is the singular value. Subsequently, the time-dependent coefficient vector \mathbf{r}_n has been computed for every time step by projecting the matrix form of the discretized governing Eq. (1) applying Galerkin Projection onto a reduced sub-space of the POD basis as follows:

$$\begin{aligned} \mathbf{A}\mathbf{z}_a &= \mathbf{f} \xrightarrow{\text{Galerkin Projection}} (\mathbf{P}^T \mathbf{A} \mathbf{P} \mathbf{r}_n) = (\mathbf{P}^T \mathbf{f}) \\ \mathbf{r}_n &= (\mathbf{P}^T \mathbf{A} \mathbf{P})^{-1} (\mathbf{P}^T \mathbf{f}) \end{aligned} \quad (27)$$

where \mathbf{A} is the stiffness matrix, \mathbf{z}_a is the hydraulic head vector, and \mathbf{f} is the force vector.

The *preComputation* application performs all the pre-requisite computations necessary for the *reducedConfinedGWFlowFOAM* solver. In the first step, it performs the SVD of \mathbf{S}_{snap} and forms the POD basis \mathbf{P} satisfying Eq. (26). Next, it calculates the inverse of the projected stiffness matrix given by the term $(\mathbf{P}^T \mathbf{A} \mathbf{P})^{-1}$ in Eq. (27).

reducedConfinedGWFlowFOAM

The *reducedConfinedGWFlowFOAM* application calculates the time-varying coefficient vector \mathbf{r}_n as expressed in Eq. (27) and subsequently the hydraulic head distribution using Eq. (22) for every time step utilizing the pre-computed matrices \mathbf{P} and $(\mathbf{P}^T \mathbf{A} \mathbf{P})^{-1}$.

The inherent parallel computing technique implemented in the OpenFOAM® framework through the process of domain decomposition employing the communication protocols of message passing interface (MPI) facilitates the applicability of *modFlowFOAM* for evaluating the hydrodynamics of regional-scale confined aquifer systems. The boundary conditions from the OpenFOAM® library have been utilized, and some problem-specific custom boundary conditions have been developed for solving various confined aquifer flow problems. The boundary conditions used in *modFlowFOAM* are listed in Table 2.

Illustrative modeling examples

This section demonstrates the applicability and performance evaluation of *modFlowFOAM* through six confined aquifer flow test cases (TC) of increasing complexity. A comparative study between the simulated results of *confinedGWFlowFOAM* and *reducedConfinedGWFlowFOAM* has been presented for the solved examples.

TC-1: Steady-state groundwater flow in a regional heterogeneous aquifer

The performance verification of the *confinedGWFlowFOAM* solver is started by solving a simple steady-state confined groundwater flow problem. In test case TC-1, *confinedGWFlowFOAM* has been applied to evaluate the steady-state hydraulic head distribution for the regional confined aquifer of Avra Valley, southern Arizona, USA. Since it is a steady-state problem, reduced-order modeling does not apply to TC-1. The field transmissivity data were available from 148 sample locations of Avra Valley in Clifton and Neuman (1982); however, five locations lie outside the prescribed boundary of the Avra Valley aquifer domain. The Avra Valley aquifer has been

Table 2 Boundary conditions utilized in *modFlowFOAM*

Boundary condition	Boundary condition type in OpenFOAM®
Specified hydraulic head boundary	<i>fixedValue</i> (inbuilt)
Specified flux boundary	<i>specifiedConstantConfinedGWFluxBC</i> (custom)
Impermeable boundary	<i>fixedGradient</i> (inbuilt)
Well-boundary	<i>pumpingConfinedBC</i> – Neumann boundary for steady flow into pumping wells (custom) <i>wellConfinedBC</i> – Dirichlet boundary for unsteady flow into pumping wells (custom)

discretized into an unstructured grid system of 8,060 prismatic elements. To specify the transmissivity for each element of the unstructured grid system based on the available field values, the random heterogeneous field generation algorithm presented by Dey and Dhar (2020) has been utilized. Voronoi tessellation of the Avra Valley aquifer domain was performed based on the 143 sampling well locations lying within the domain boundary. The generated Voronoi polygons, alongside the corresponding transmissivity values, are displayed in Fig. 1. The experimental semivariogram is calculated utilizing the natural logarithmic values of the measured transmissivities. A power-law model is fitted to the experimental semivariogram with parameters $c=3.5 \times 10^{-3}$ and $\omega=0.6$ (c and ω are the power-law constant and exponent, respectively). Applying the random heterogeneous field generation algorithm, 10^3 Monte Carlo realizations of the transmissivity field for the Avra Valley aquifer have been generated. Figure 2 displays the contour plot of the mean log transmissivity field generated for the Avra Valley aquifer.

A detailed description of the climatic, geological, and hydrogeological features of the Avra Valley can be found in Clifton and Neuman (1982). The Avra Valley aquifer is bounded by three types of boundaries—constant hydraulic head boundary, constant flux boundary, and impermeable boundary (Clifton and Neuman 1982). The recharge from rain infiltration, which was very low due to the prevailing arid climatic conditions, has been ignored (Clifton and Neuman 1982). Surface recharge through seepage from streams, sewage effluents, and irrigation return flows was insignificant and did not contribute to groundwater development (Clifton and Neuman 1982). The boundary specifications considered for modeling the steady-state groundwater characteristics of the Avra Valley aquifer are presented in Fig. 3. An approximate location of the constant flux boundary was selected based on the domain boundary specifications presented in Clifton and Neuman (1982). Moreover, the hydraulic head to be specified at the bottom constant head boundary of the aquifer was not mentioned. Therefore, an approximate hydraulic head value of 640.08 m has been assumed on that boundary based on the available hydraulic head distribution data presented in Clifton and Neuman (1982).

The hydraulic heads estimated by *confinedGWFlowFOAM* have been compared with those computed deterministically by Clifton and Neuman (1982) with the aid of kriged transmissivities. Figure 4 displays the comparison of the hydraulic head contours. The head difference was sufficiently low in the northern region of the Avra Valley aquifer, where the estimated hydraulic heads differed by less than 1.5 m for most of the region. It is evident from Fig. 4 that there are significant deviations between the estimated hydraulic heads for the southern region of the Avra Valley aquifer. This is primarily attributed to the approximations of locating the constant flux boundary and specifying the hydraulic head at the bottom constant head boundary. While

generating the transmissivity field, the conditioning transmissivity values from two wells located outside the aquifer domain close to the left impermeable boundary were omitted. This has significantly affected the estimated transmissivity field near that boundary. Omission of the conditioning transmissivity values is the possible cause behind large deviations in simulated hydraulic heads observed in the proximity of the left impermeable boundary.

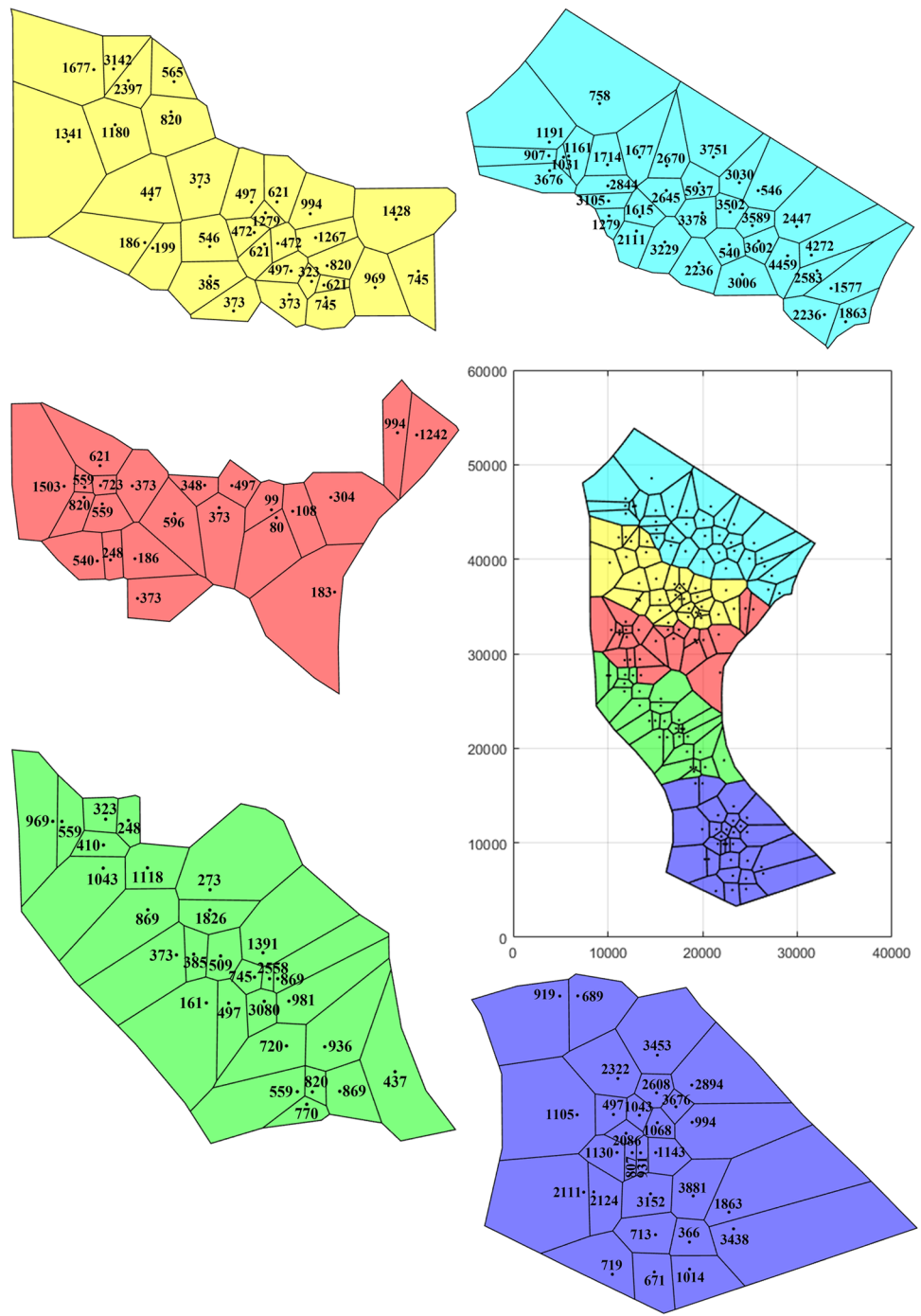
TC-2: Quasi-steady groundwater flow in a homogeneous synthetic confined aquifer (single pumping well)

In TC-2, a 2D synthetic square-shaped confined aquifer of sides 3,200 m and thickness 50 m was considered (Tsai 2006; Dey and Dhar 2020), as shown in Fig. 5. The aquifer is homogeneous with constant values of $K_x=K_y=50$ m/day and $S_s=10^{-4}$ /m. An initial hydraulic head of 50 m has been considered. The domain boundaries are Dirichlet boundaries with a specified constant hydraulic head of 50 m. A pumping well of radius 0.1 m pumping at a constant rate of 10^4 m³/day is located at the center of the aquifer. The hydraulic head distribution in the confined aquifer at the end of the 15 days pumping test simulated with *confinedGWFlowFOAM* has been compared with the numerical results presented in Dey and Dhar (2020).

For modeling TC-2, *confinedGWFlowFOAM* requires representation of the well-boundary at a radial distance equal to the finite well radius (Fig. 5). As the length scales of the well and the domain differ significantly, high grid refinement is essential around the well-boundary to avoid issues related to grid orthogonality, aspect ratio, and skewness. This results in an unstructured grid system with 12,140 prismatic elements, which is comparatively higher than those generated for the grid system (5,516 elements) used in Dey and Dhar (2020). The well-boundary is subjected to a specified outward flux equal to the pumping rate per unit circumferential length of the boundary.

The performance of *confinedGWFlowFOAM* has been evaluated against the simulation results of MODFLOW-USG. The simulations are carried out using the WEL package on a square-grid system in MODFLOW-USG. It has been observed that the drawdown values within the pumping well are inconsistent with changing grid dimensions. This can be attributed to the concept of effective well radius considered in MODFLOW-USG, which changes with varying grid dimensions. Grid refinement has been applied around the well using MODFLOW-LGR so that the calculated effective well radius approaches the actual finite well radius. The *confinedGWFlowFOAM* results closely agree with the results of Dey and Dhar (2020), as both models perform the simulations with the actual finite well radius. On the other hand, the *confinedGWFlowFOAM* results are in the acceptable range of

Fig. 1 Voronoi tessellation of the Avra Valley aquifer domain with 143 well locations (black dots) and the corresponding field transmissivities measured in m^2/day . Length units are in meters



MODFLOW-USG results (Table 3) only when the effective well radius is approximately equal to the actual finite well radius. Figure 6 claims that *confinedGWFlowFOAM* offers better grid-convergence than MODFLOW-USG using the WEL package. A comparison of the drawdown at the pumping well location calculated via MODFLOW-USG (Dey and Dhar 2020) and *confinedGWFlowFOAM* for different grid dimensions is shown in Table 3, along with the respective CPU computation times.

Figure 7 compares the time evolution of drawdown at the well location estimated by *confinedGWFlowFOAM* with the results of Dey and Dhar (2020). Since the methodologies adopted by the two models for estimating the well drawdown are different, the steady-state drawdowns differ by 0.28 m. However, steady-state conditions are attained almost simultaneously for both models approximately after 5 days from the commencement of the pumping operation. Figure 8 displays the contour plots of the drawdown

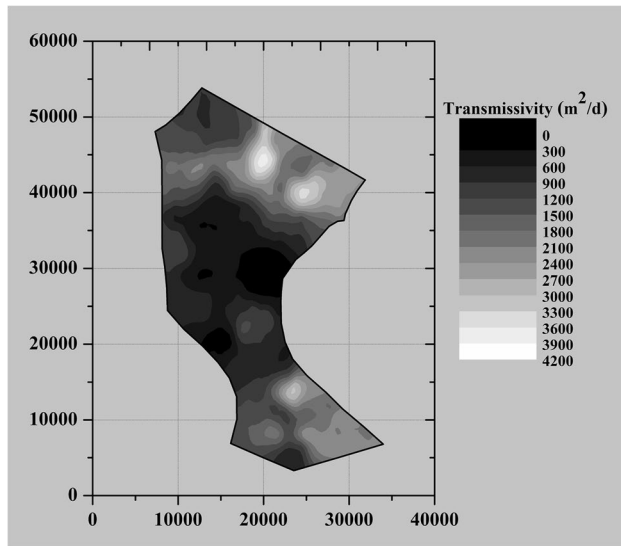


Fig. 2 Contour diagram of estimated log transmissivity, $\ln(T)$, distribution for the Avra Valley aquifer domain. Length units are in meters

distribution for the confined aquifer at the end of the 15 days pumping test simulated by Dey and Dhar (2020) and *confinedGWFlowFOAM*. Owing to the differences in the adopted methodologies for solving point source/sink singularity, the drawdown contours vary within a small neighborhood surrounding the pumping well. Moving farther away from the well, the drawdown contours start overlapping and match perfectly with each other.

For reduced-order modeling with *reducedConfinedGWFlowFOAM*, 12 snapshots have been captured at an increased pumping rate of $10^5 \text{ m}^3/\text{day}$ to obtain a profound response from every part of the aquifer. At the onset of the pumping operation, the flow dynamics change rapidly, requiring more snapshots during the early simulation time. Accordingly, $\tilde{c}_s = 5$ and $T_s = 5$ days have been assumed for calculating t_s . The POD basis computed from the snapshot matrix consists of 11 vectors. Therefore, for every time step, the dimension of the problem reduces from 12,140 to 11. As a result, a speedup of 470 times has been achieved by applying *reducedConfinedGWFlowFOAM* relative to *confinedGWFlowFOAM* for the solution of TC-2. The hydraulic head distribution estimated by *reducedConfinedGWFlowFOAM* closely agrees with the results of *confinedGWFlowFOAM* with maximum absolute error ($\text{maxAE} = 5.5 \times 10^{-3} \text{ m}$). The drawdown contours at the end of the 15 days pumping test simulated by *confinedGWFlowFOAM* and *reducedConfinedGWFlowFOAM* have been compared in Fig. 8b. The other error statistic parameters listed in Table 5 determine the accuracy of *reducedConfinedGWFlowFOAM* and justify its applicability as an alternative for *confinedGWFlowFOAM*.

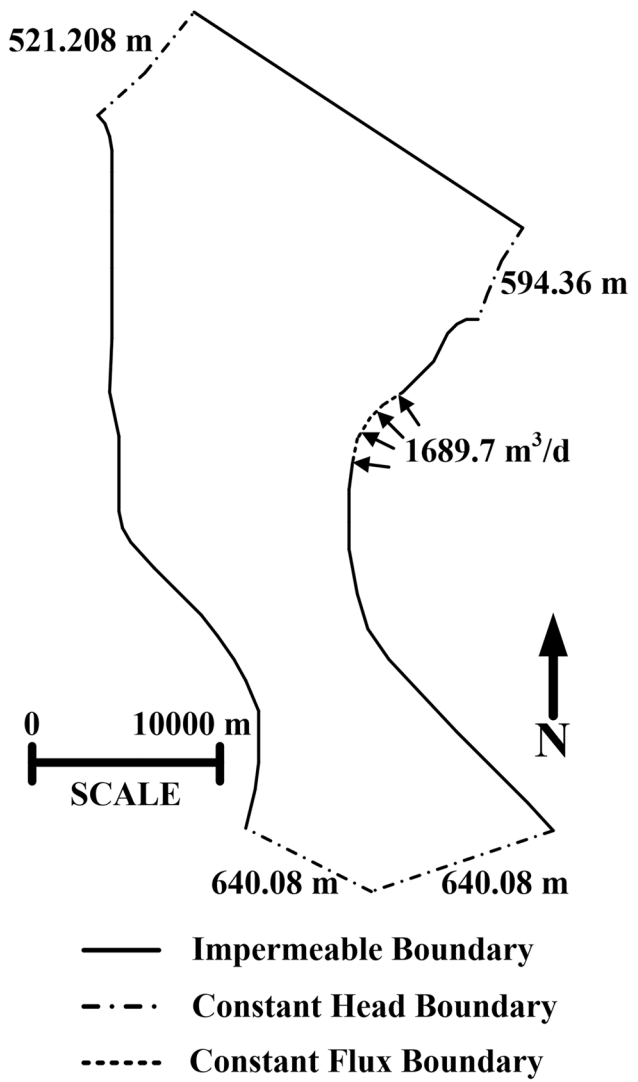


Fig. 3 Avra Valley aquifer alongside the boundary specifications

TC-3: Quasi-steady groundwater flow in a heterogeneous synthetic confined aquifer (single pumping well)

In this subsection, TC-2 has been solved, assuming the confined aquifer to be heterogeneous, as done by Dey and Dhar (2020). In this problem, pumping has been done at a constant rate of $10^4 \text{ m}^3/\text{day}$ for 30 days. The hydraulic conductivity field has been generated following the algorithm presented by Dey and Dhar (2020), as shown in Fig. 9. The hydraulic head distributions estimated by *confinedGWFlowFOAM* at the end of the 30 days pumping test alongside the results of Dey and Dhar (2020) have been presented in Fig. 10. Similar to TC-2, the drawdown contours in the proximity of the well vary from each other, whereas at greater distances match perfectly with each other. *confinedGWFlowFOAM* perfectly captures the effect

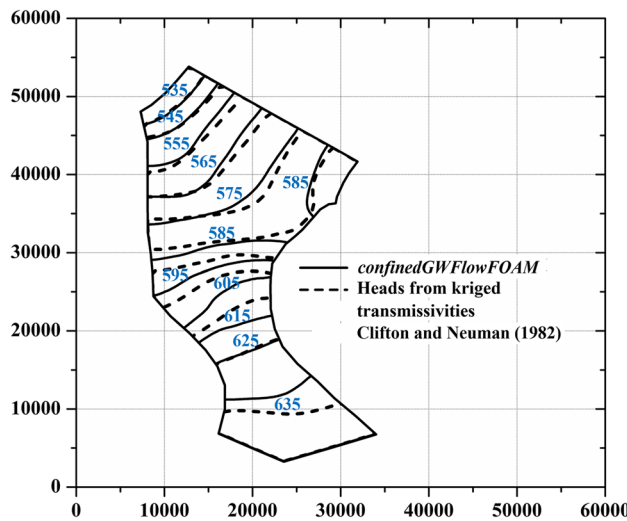


Fig. 4 Comparison between the hydraulic head contours for Avra Valley aquifer simulated by *confinedGWFlowFOAM* and Clifton and Neuman (1982). Length units are in meters

of random heterogeneity on the movement of water through the confined aquifer. In the regions around the bottom-left and top-right boundaries, where the hydraulic conductivity is low, the steady-state drawdown contours are elliptic in shape, with the major axis along the diagonal joining the bottom-left and top-right corners of the domain. This signifies that greater drawdown results in zones of low permeability; however, the highly permeable regions near the bottom-right and top-left boundaries of the aquifer immediately get replenished by water entering through the constant head boundaries. This results in relatively lesser drawdown and, therefore, flattened drawdown contours are observed around those boundaries. The drawdown

estimated by *confinedGWFlowFOAM* at the pumping well location differs by 0.16 m from the results of Dey and Dhar (2020).

For reduced-order modeling, 20 snapshots have been recorded within a period of 6 days from the commencement of the pumping operation at an enhanced rate of 10^5 m³/day. The ‘snapshot time-set’ has been calculated with $c = 5$ and $T_s = 5$ days. In the subsequent step, SVD of the snapshot matrix was performed, recognizing 16 dominant modes that constitute the POD basis. Applying *reducedConfinedGWFlowFOAM*, the hydraulic head distribution within the confined aquifer system has been evaluated after 30 days of constant pumping with $\text{maxAE} = 1.47 \times 10^{-2}$ m and 121 times reduction in computation time relative to *confinedGWFlowFOAM*. The assignment of variable hydraulic conductivity value for each element of the unstructured grid system has significantly reduced the expected computation speedup with *reducedConfinedGWFlowFOAM* compared to TC-2. However, the error statistic parameters (Table 5) reveal that incorporating heterogeneity of the conductivity field does not affect the solution accuracy of *reducedConfinedGWFlowFOAM*. A comparison of the drawdown contours simulated by *confinedGWFlowFOAM* and *reducedConfinedGWFlowFOAM* after 30 days of constant pumping has been presented in Fig. 10b.

TC-4: Quasi-steady groundwater flow in a heterogeneous synthetic confined aquifer (multiple pumping wells)

In TC-4, the hydrodynamics of the heterogeneous confined aquifer illustrated in TC-3 has been solved, considering three pumping wells to be pumping simultaneously at a constant rate of 5×10^3 m³/day throughout the 90 days pumping test.

Fig. 5 Schematic diagram showing the domain of TC-2 alongside the unstructured grid system used for *confinedGWFlowFOAM*

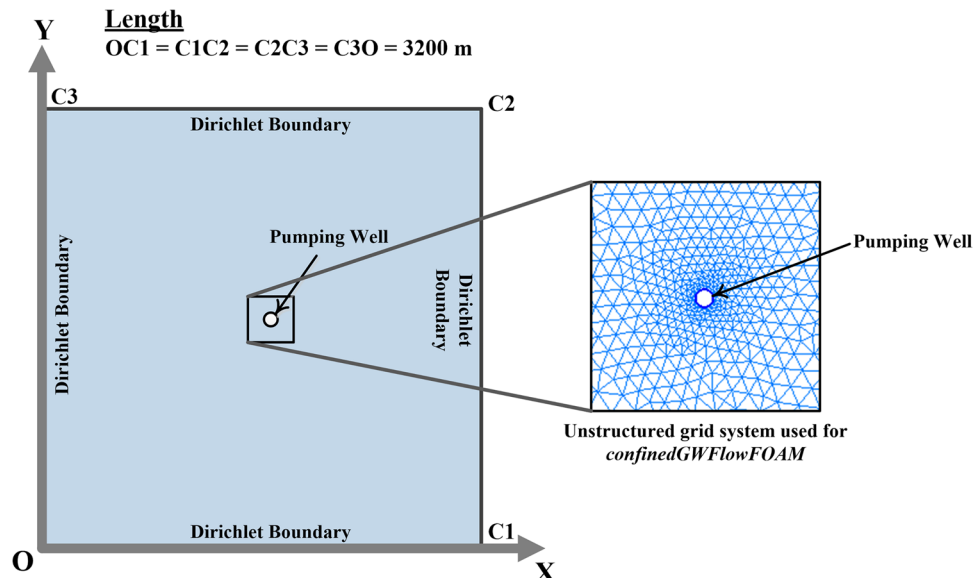


Table 3 Comparison among well drawdown results of MODFLOW, Dey and Dhar (2020), and *confinedGWFlowFOAM* for different grid dimensions

	Simulation model used	No. of elements	Effective well radius (m)	Drawdown at well location (m)	CPU time per iteration (s)
MODFLOW-USG	2,601	12.6	3.13	7.98×10^{-3}	
	10,201	6.3	3.57	8.46×10^{-3}	
	40,401	3.2	3.94	2.14×10^{-2}	
MODFLOW-LGR	2,601	0.5	5.11	1.8×10^{-2}	
	10,201	0.25	5.53	2.18×10^{-2}	
	40,401	0.1	6.01	4.92×10^{-2}	
Dey and Dhar (2020)	5,516	0.1	5.93	2.32×10^{-3}	
	22,222	0.1	5.89	4.97×10^{-2}	
<i>confinedGWFlowFOAM</i>	12,140	0.1	6.21	2.17×10^{-2}	
	55,548	0.1	6.20	4.96×10^{-1}	

The thickness of the confined aquifer is assumed to be 100 m. The complexity of the problem has been increased by considering only the left boundary of the aquifer to be a Dirichlet boundary with a constant hydraulic head of 100 m. The other three boundaries are assumed impervious (Fig. 11). A uniform hydraulic head of 100 m has been assumed throughout the aquifer at the start of the pumping test. The aquifer has been discretized into an unstructured grid system of 26,060 prismatic elements. The hydraulic conductivity field utilized for the flow simulation is presented in Fig. 9. The drawdown contours estimated by *confinedGWFlowFOAM* have been compared with the results of Dey and Dhar (2020) after 90 days of pumping (Fig. 12). As the approaches adopted for modeling a point-source singularity differ, the drawdown contours estimated by them are nonoverlapping in the neighborhood of the pumping wells. Since the impermeable boundaries do not allow the entrance of water into the aquifer for replenishment, differences in estimated drawdown have been observed along

these boundaries between the two models. However, due to the Dirichlet boundary on the left, the drawdown contours show a perfect match close to that boundary.

Three sets of 30 snapshots have been captured for performing reduced-order modeling as three pumping wells operate simultaneously. The snapshot sets were merged to form the final snapshot matrix. For each snapshot set, one pumping well was operated at an enhanced rate of $10^5 \text{ m}^3/\text{day}$, while the others were kept inoperative. For capturing all three snapshot sets, t_s was calculated assuming $\tilde{c} = 5$ and $T_s = 6$ days. The POD basis computed from the final snapshot matrix comprises 53 dominant vectors. Based on the pattern of aquifer flow dynamics identified by the POD basis, *reducedConfinedGWFlowFOAM* estimates the hydraulic head distribution after 90 days of pumping with $\text{maxAE} = 5.27 \times 10^{-2} \text{ m}$ relative to *confinedGWFlowFOAM*. Moreover, an approximate gain of 764 times in computation speed has been accomplished with *reducedConfinedGWFlowFOAM* compared to *confinedGWFlowFOAM*.

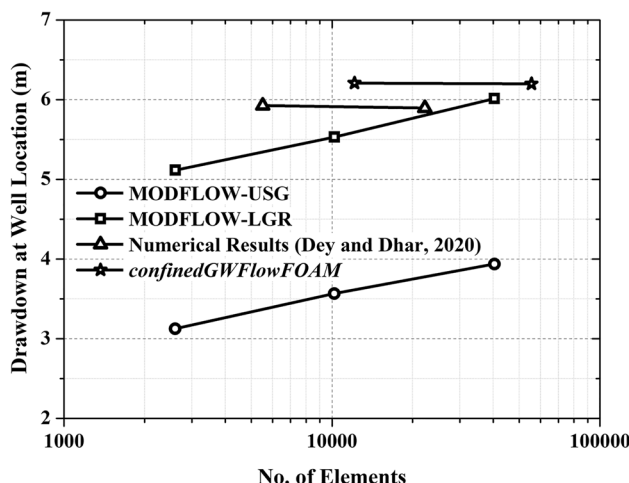


Fig. 6 Comparison of grid-convergence among the results of MODFLOW, Dey and Dhar (2020), and *confinedGWFlowFOAM*

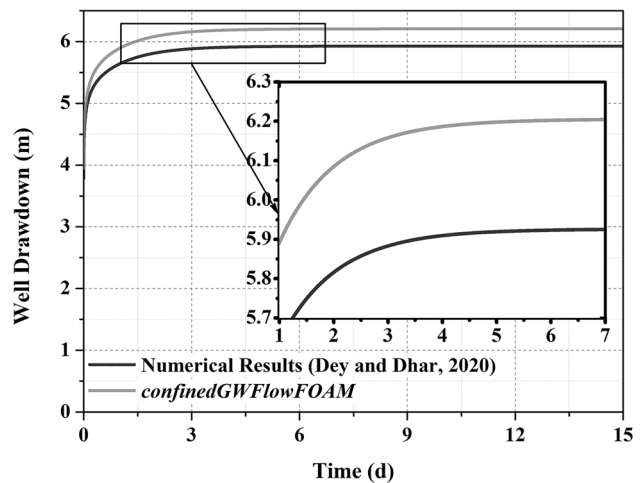


Fig. 7 Comparison of well drawdown estimated by Dey and Dhar (2020) and *confinedGWFlowFOAM* for TC-2

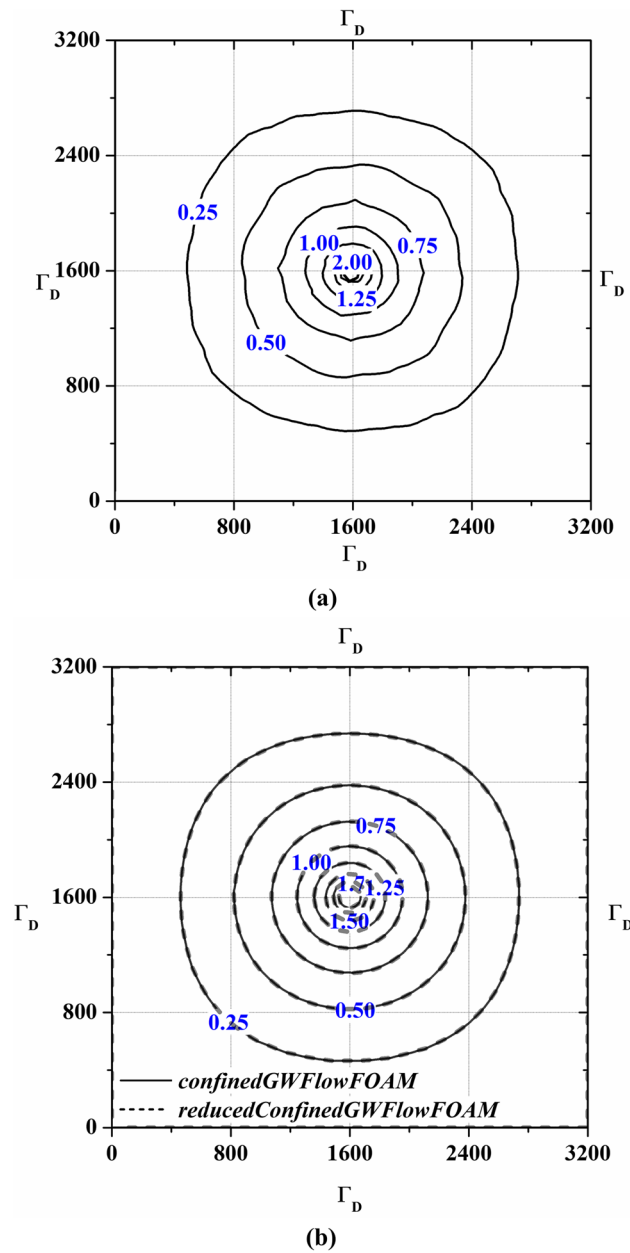


Fig. 8 Drawdown contours at the end of 15 days pumping test estimated by **a** Dey and Dhar (2020); **b** *confinedGWFlowFOAM* and *reducedConfinedGWFlowFOAM* for TC-2. Length units are in meters

Figure 12b compares the drawdown contours at the end of the 90 days pumping test simulated by *confinedGWFlowFOAM* and *reducedConfinedGWFlowFOAM*. Although the maximum absolute error is slightly higher, ~88% of the domain exhibits absolute estimation error values less than 10^{-3} m. The other error statistic parameters presented in Table 5 confirm the accuracy of *reducedConfinedGWFlowFOAM*, thereby ensuring its application as a potential alternative to *confinedGWFlowFOAM* for multiple-well and complex boundary test problems.

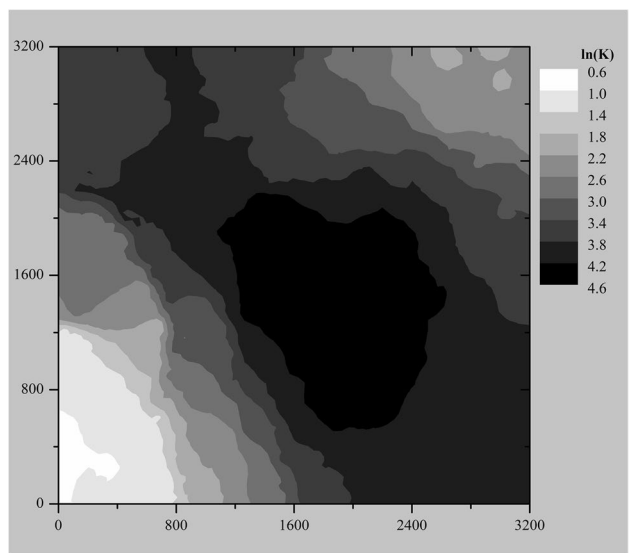


Fig. 9 Contour diagram of estimated $\ln(K)$ distribution for the synthetic confined aquifer domain for TC-3 and TC-4. Length units are in meters

TC-5: Lohman problem

A significant advantage of *confinedGWFlowFOAM* is that it can be applied to well-hydraulics problems subjected to unsteady flow into fully or partially penetrating wells in confined aquifers. In TC-5, the hypothetical confined aquifer system described in Lohman (1972) has been considered as an example of a system subjected to unsteady radial flow into a pumping well without vertical movement. This test problem has also been used for testing, evaluating, and demonstrating the MNW2 package for MODFLOW (Konikow et al. 2009). The synthetic confined aquifer is square-shaped, with sides of 91,440 m (300,000 ft) and a thickness of 30.48 m (100 ft), as shown in Fig. 13. The aquifer has isotropic and homogeneous properties with $K_z = K_r = 42.67$ m/day (140 ft/day) and $S_s = 6.56 \times 10^{-4}$ m (2×10^{-6} ft). A pumping well of radius 0.3018 m (0.99 ft) and completely penetrating the saturated thickness is positioned at the center of the aquifer. The pumping well operates at a constant rate of 2,718.42 m³/day (96,000 ft³/day) for 100 days. The confined aquifer is assumed to be impervious on all four boundaries with an initial hydraulic head distribution of 30.48 m.

As shown in Fig. 13, the well-boundary has been considered to be located at a radial distance of 0.5 m from the center of the pumping well. An unstructured grid system consisting of 25,822 prismatic elements has been generated to model the unsteady flow dynamics in the aquifer. To examine the reliability of the well-boundary approach for modeling confined aquifer hydrodynamics due to unsteady flow into pumping wells, the drawdowns estimated by *confinedGWFlowFOAM* at the pumping well

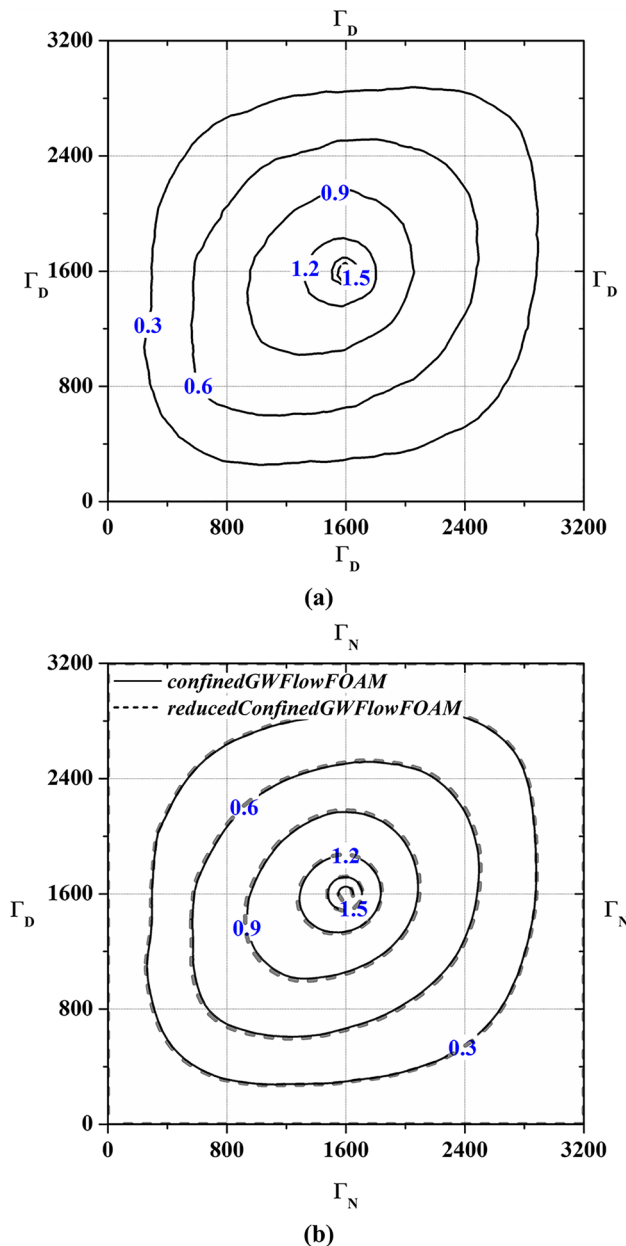


Fig. 10 Drawdown contours at the end of 30 days pumping test estimated by **a** Dey and Dhar (2020); **b** *confinedGWFlowFOAM* and *reducedConfinedGWFlowFOAM* for TC-3. Length units are in meters

and also at radial distances of 1.524 m (5 ft), 3.048 m (10 ft), 6.096 m (20 ft), 60.96 m (200 ft), and 121.92 m (400 ft) have been compared with the 2D numerical results of MODFLOW (MNW2 package) presented in Konikow et al. (2009) and 3D results of *subsurfaceFlowFOAM* (Dey and Dhar 2022). Three simulations have been performed with *confinedGWFlowFOAM* considering the well-boundary at radial distances of 0.5, 5, and 50 m from the center of the pumping well. Figure 14 reveals that the *confinedGWFlowFOAM* results are in excellent agreement with the

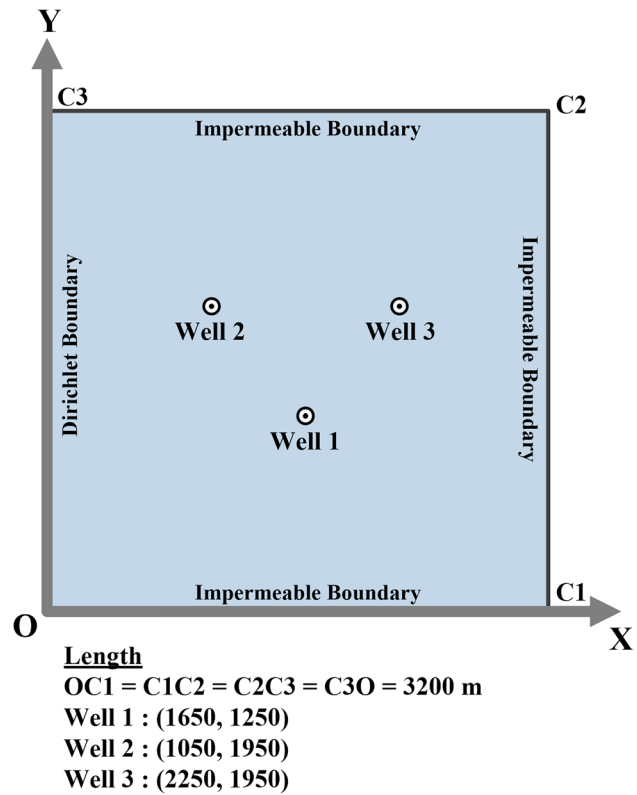


Fig. 11 Schematic diagram showing the domain alongside the boundary conditions considered for TC-4

numerical results of MODFLOW (MNW2 package) and *subsurfaceFlowFOAM*.

In this section, low-dimensional modeling of the Lohman problem has been attempted by applying *reducedConfinedGWFlowFOAM*. The pattern identification procedure is challenging since it is an unsteady flow problem. Within the span of 30 days, 20 snapshots have been captured from the commencement of the pumping operation at 6 times the actual pumping rate considered for the problem. The value of c assumed for calculating t_s is 5. A POD basis consisting of 16 vectors has been formed on the orthonormalization of the snapshot matrix. With the formed POD basis, *reducedConfinedGWFlowFOAM* replicates the hydraulic head distribution estimated by *confinedGWFlowFOAM* after 100 days of constant pumping with $\text{maxAE} = 1.37 \times 10^{-2} \text{ m}$. Figure 15 shows the comparison of drawdown contours at the end of 100 days pumping test estimated by *confinedGWFlowFOAM* and *reducedConfinedGWFlowFOAM*. The error statistic parameters presented in Table 5 also speak about the accuracy of the *reducedConfinedGWFlowFOAM* and justify its applicability for solving unsteady flow into pumping wells in confined aquifer systems.

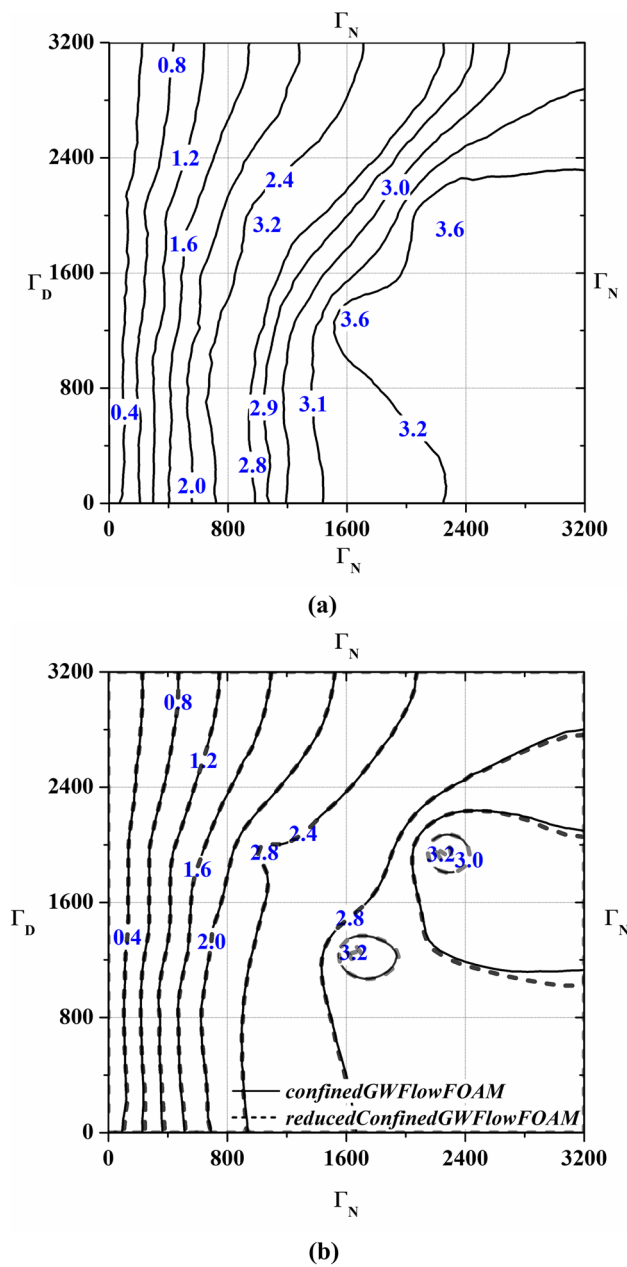


Fig. 12 Drawdown contours at the end of 90 days pumping test estimated by **a** Dey and Dhar (2020); **b** *confinedGWFlowFOAM* and *reducedConfinedGWFlowFOAM* for TC-4. Length units are in meters

TC-5A: Lohman problem for partially penetrating wells

The partially penetrating pumping wells are open to a fraction of the thickness of the confined aquifer, and hence the flow characteristics differ from those in fully penetrating wells. A vertical flow component is dominant in the vicinity of the partially penetrating wells, as the flowlines have to converge at the ends of the well-screen. This stretches the flow path of water entering the well. In anisotropic aquifer systems, vertical hydraulic conductivity value is generally very low

compared to the same in the radial direction, which causes increased resistance to the flowlines that converge at the ends of the well-screen. Hence, a more significant drawdown is observed within a partially penetrating pumping well than in a fully penetrating one where the flow is ideally horizontal. Partially penetrating wells are identified by the corresponding partial penetration fraction α_p , which is defined as the fraction of the thickness of the confined aquifer to which the pumping well is open and can be expressed as follows:

$$\alpha_p = \frac{l - d}{b} \quad (28)$$

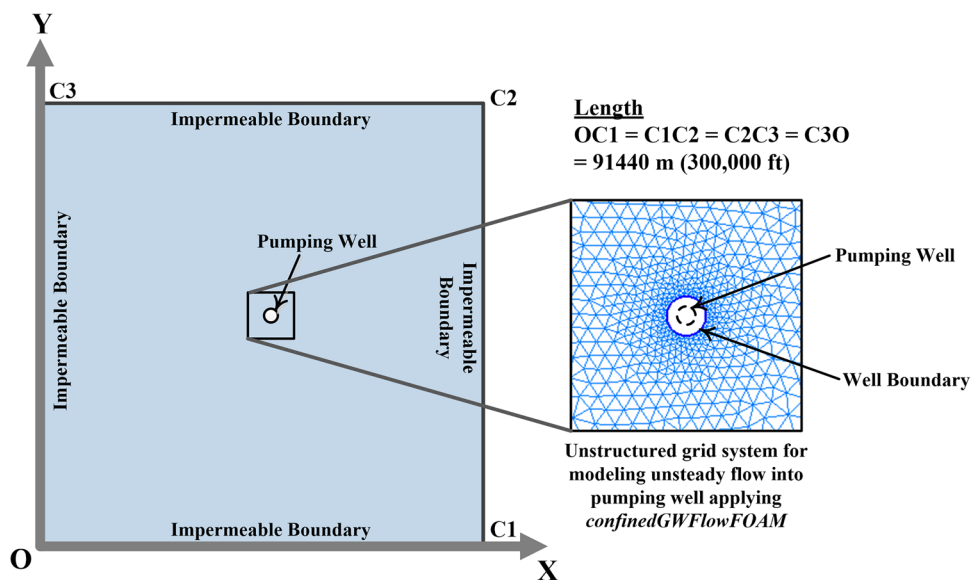
To model the effects of partial penetration of pumping wells in a confined aquifer applying *confinedGWFlowFOAM*, simulations have been performed with $\alpha_p = 0.1, 0.25, 0.5$, and 0.75 (Fig. 16) for the hypothetical confined aquifer system described in TC-5. The results have been compared with the 3D model simulations performed with *subsurfaceFlowFOAM* (Dey and Dhar 2022) in Fig. 17. For the time scale adopted in these simulations, the additional well drawdown due to partial penetration has been constant with time; hence, in Fig. 17, the semi-log plots of the drawdowns estimated by *confinedGWFlowFOAM* at the pumping well for different values of α_p represent a family of parallel straight lines. It has been inferred that the effect of partial penetration is less when the α_p value is close to 1.0, which increases rapidly upon lowering the value of α_p . Figure 17 shows that *confinedGWFlowFOAM* successfully simulates the effects of vertical flow gradients and can be claimed to be a 3D-equivalent model for 2D confined groundwater flow.

Vertical flow gradients arising from partial penetration of pumping wells affect the drawdown in the aquifer in the proximity of the well. Following Eq. (5), the well-boundary has been considered at a radial distance of 50 m for the simulations with partially penetrating wells. The flow becomes horizontal beyond the well-boundary; therefore, Eq. (1) governing confined groundwater flow becomes applicable. The estimated drawdown at the well-boundary is 2.2109 m for all the considered values of α_p , signifying that the effect of partial penetration completely vanishes at the well-boundary. Moreover, the drawdowns simulated by *confinedGWFlowFOAM* for the fully penetrating pumping well at a radial distance of 50 m are 2.2078 and 2.2099 m, considering the well-boundary at radial distances of 0.5 and 5 m, respectively. The results justify the suitability of the proposed well-boundary approach and the capability of *confinedGWFlowFOAM* in modeling unsteady flow into partially penetrating pumping wells in a confined aquifer system.

TC-5B: Lohman problem with a partially penetrating well ($\alpha_p = 0.5$) for different vertical positions of the well-screen

This subsection performs a comparative study on the vertical positions of the open interval for a partially penetrating

Fig. 13 Schematic diagram showing the domain alongside the unstructured grid system generated for modeling unsteady flow into the pumping well applying *confinedGWFlowFOAM* for TC-5



pumping well with $\alpha_p = 0.5$. Three different locations of the open interval have been considered (wells A, B and C), as shown in Fig. 18. The semi-log plots of the drawdowns computed by *confinedGWFlowFOAM* and *subsurfaceFlowFOAM* for the different vertical positions of the open interval are displayed in Fig. 19. Essentially, nonuniform flow occurs into a partially penetrating well as the flowlines, from above and below the well-screen, converge at the top and bottom ends of the screen (Petersen et al. 1955). In well A, where the top of the well-screen is adjacent to the top confining layer, the deviation of the flowlines is nearer the bottom

end of the well-screen (Fig. 20b), increasing the magnitude of the vertical flow gradients, resulting in a significantly greater drawdown within the pumping well. The deviation of flowlines near the top and bottom ends of the well-screen is considerably less when the screen is located some distance away from both the confining layers (Fig. 20c), as has been the case for wells B and C. Hence, the drawdowns in wells B and C are comparatively less than in well A for the same pumping rate; however, a minimum drawdown in a fully penetrating well is observed as the flow is uniform and the resulting flowlines are parallel, ensuring horizontal flow.

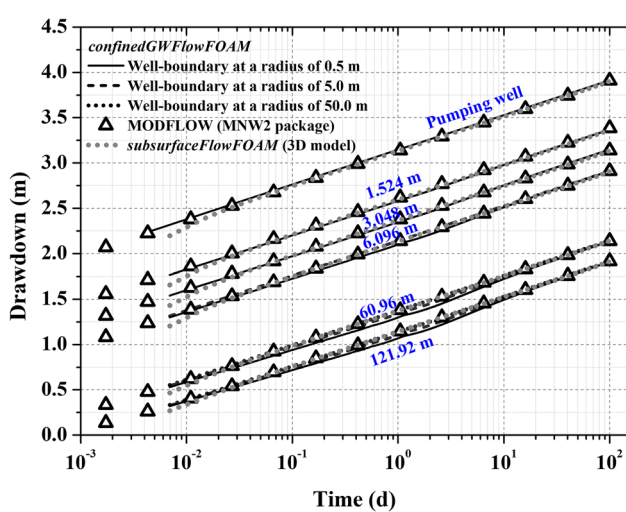


Fig. 14 Comparison of the drawdowns estimated by *confinedGWFlowFOAM*, MODFLOW (MNW2 package), and *subsurfaceFlowFOAM* (3D model) at the pumping well and at selected radial distances with the well-boundary located at 0.5, 5, and 50 m from the center of the pumping well for TC-5

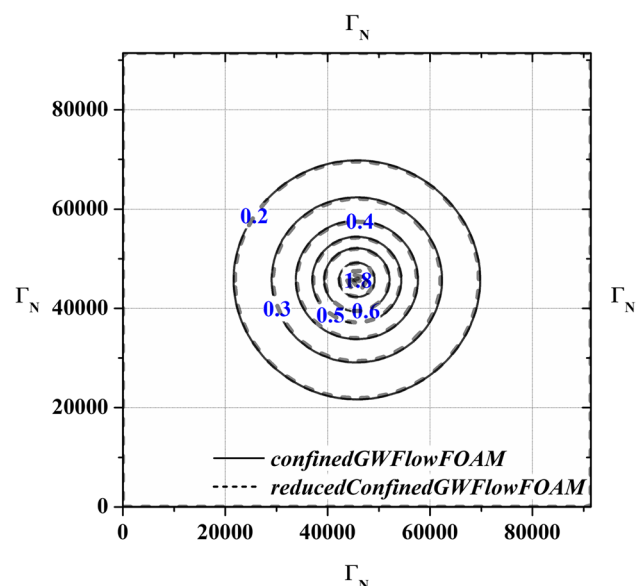


Fig. 15 Comparison of drawdown contours at the end of 100 days pumping test estimated by *confinedGWFlowFOAM* and *reducedConfinedGWFlowFOAM* for TC-5. Length units are in meters

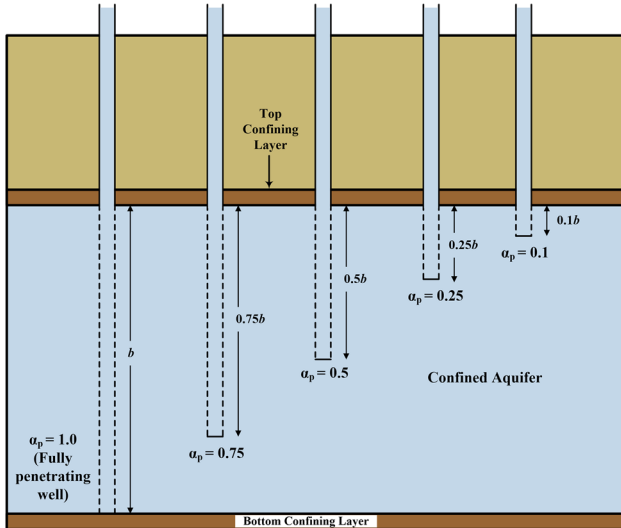


Fig. 16 Schematic cross-sectional diagram showing partially penetrating pumping wells with different values of α_p in a confined aquifer

TC-6: Quasi-steady groundwater flow in a heterogeneous regional-scale real confined aquifer (multiple pumping wells)

The applicability of *modFlowFOAM* to large-scale regional aquifer systems has been validated in TC-6. The groundwater flow in a confined aquifer in the Oristano plain located in west-central Sardinia, Italy, has been simulated (Cau et al. 2002; Siade et al. 2012; Ushijima et al. 2013). The aquifer is surrounded on all sides by Dirichlet boundaries and divided into seven hydrologic zones (Fig. 21), whose properties are listed in Table 4. Six pumping wells of diameter 0.1 m extract groundwater

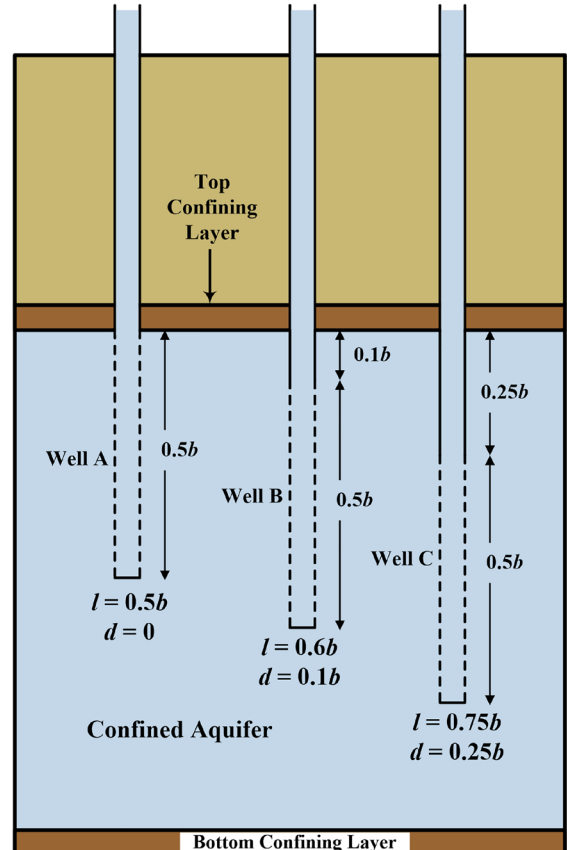


Fig. 18 Schematic cross-sectional diagram showing the vertical positions of the open interval for a partially penetrating pumping well with $\alpha_p = 0.5$ in a confined aquifer

at a rate of $10^3 \text{ m}^3/\text{day}$ for 100 days. A hydraulic head of 110 m has been assumed to be distributed throughout the aquifer at the start of the simulation.

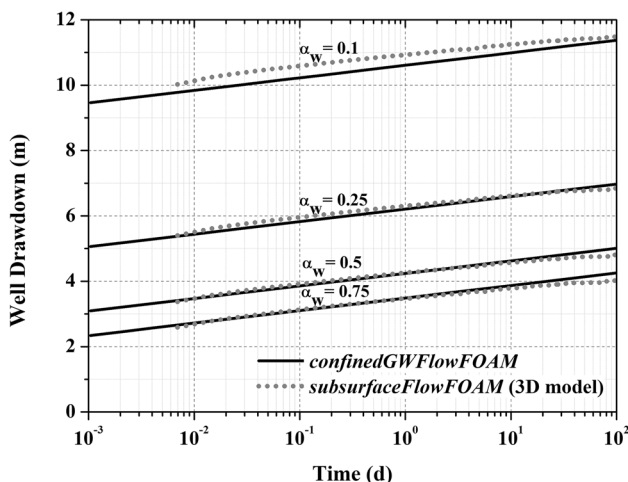


Fig. 17 Comparison of the well drawdowns estimated by *confinedGWFlowFOAM* and *subsurfaceFlowFOAM* (3D model) for different values of α_p

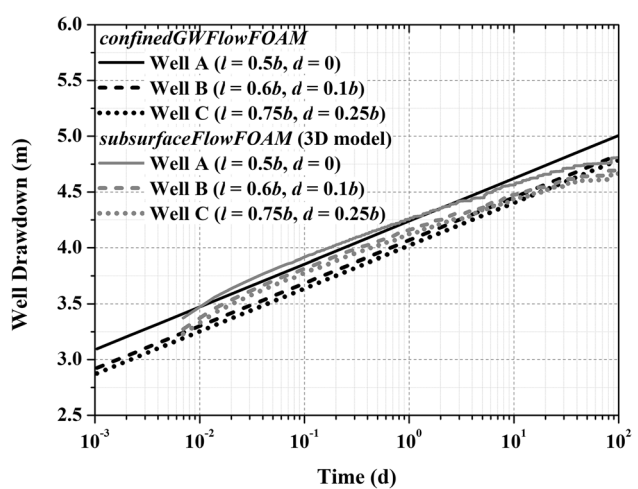


Fig. 19 Comparison of the well drawdowns estimated by *confinedGWFlowFOAM* and *subsurfaceFlowFOAM* (3D model) for different vertical positions of the open interval for a partially penetrating pumping well with $\alpha_p = 0.5$

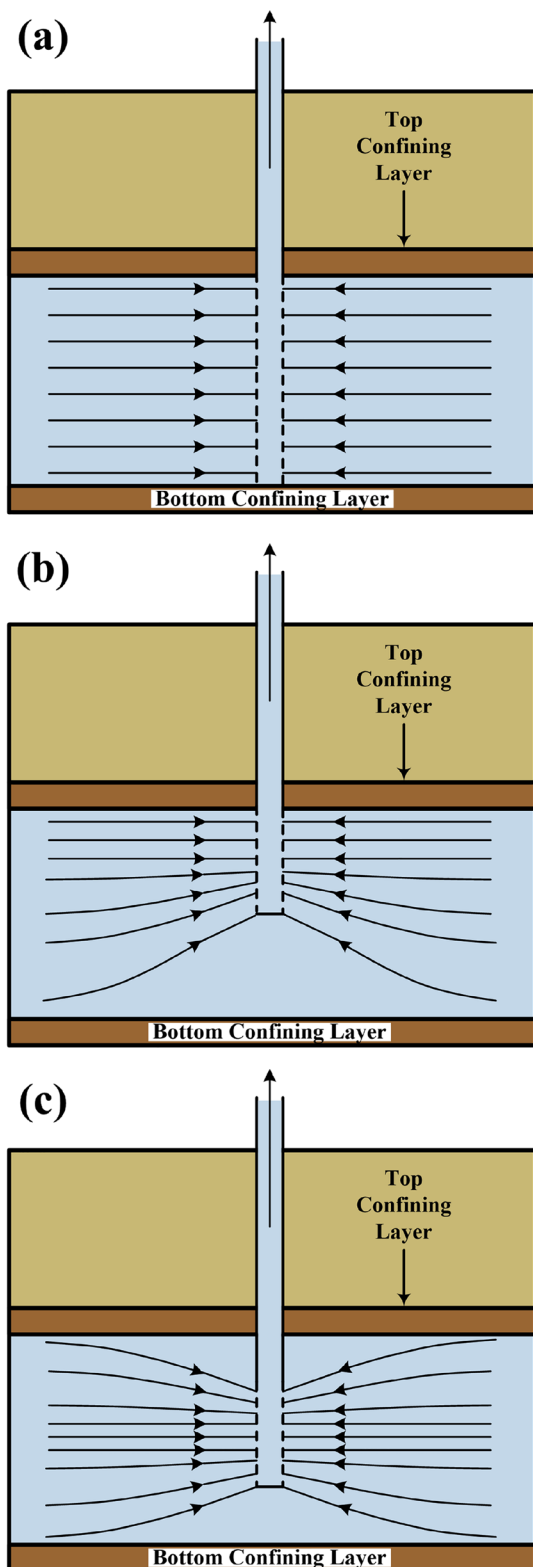


Fig. 20 Schematic diagram of flowlines in a confined aquifer subjected to pumping through **a** a fully penetrating pumping well, **b** a partially penetrating pumping well where the top of the well-screen is adjacent to the top confining layer, and **c** a partially penetrating pumping well where both the top and bottom ends of the well-screen are some distance away from the adjacent confining layers

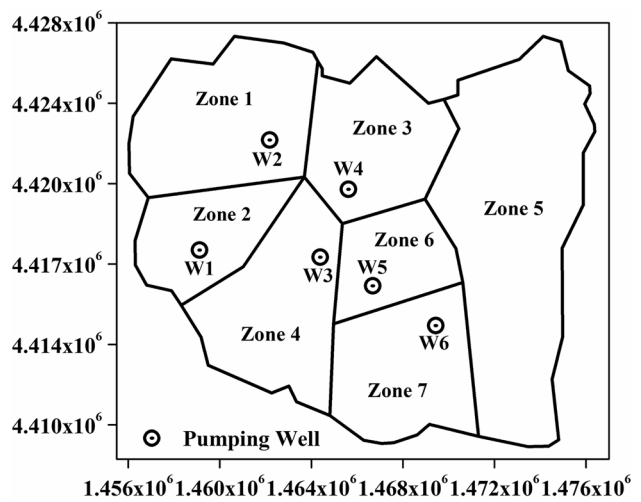


Fig. 21 Oristano Aquifer domain alongside the hydrologic zones and the pumping wells. Length units are in meters

The groundwater flow simulation for the Oristano aquifer is performed on an unstructured grid system of 12,602 prismatic elements. For reduced-order modeling, six sets of snapshots were captured to identify the effects of pumping from each well separately on the groundwater dynamics of the Oristano aquifer. Each set has 25 snapshots at t_s calculated with $\tilde{c} = 6$ and $T_s = 30$ days with the active pumping well operating at an enhanced rate of $2 \times 10^3 \text{ m}^3/\text{day}$. A POD basis was formed with the 145 dominant vectors after performing SVD of the final snapshot matrix. A comparison of the drawdown contours estimated by *confinedGWFlowFOAM* and *reducedConfinedGWFlowFOAM* at the end of 100 days has been displayed in Fig. 22. The *reducedConfinedGWFlowFOAM* solver simulates the hydraulic head distribution in the confined aquifer system of the Oristano plain 165 times faster than *confinedGWFlowFOAM*. The error statistic parameters listed in Table 5 claim the acceptability of *reducedConfinedGWFlowFOAM* as an alternative to *confinedGWFlowFOAM* for modeling confined groundwater flow in large-scale regional aquifer systems.

Table 4 Hydraulic zone properties of the Oristano plain aquifer

Zone	$K_x = K_y$ (m/day)	S_s (1/m)	b (m)
1	5	1.2×10^{-5}	100
2	10	2.7×10^{-5}	85
3	7	1.0×10^{-5}	110
4	15	1.7×10^{-5}	100
5	12	2.1×10^{-5}	96
6	9	3.4×10^{-5}	105
7	11	1.0×10^{-5}	104

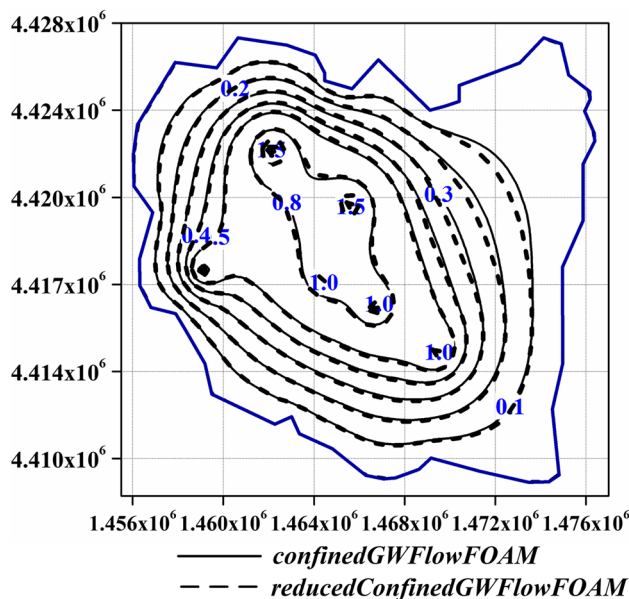


Fig. 22 Comparison of drawdown contours at the end of 100 days pumping test estimated by *confinedGWFlowFOAM* and *reducedConfinedGWFlowFOAM* for the Oristano aquifer considered in TC-6. Length units are in meters

Discussion

The results of *confinedGWFlowFOAM* for the solved test examples have been observed to overcome the issues of grid-convergence faced by MODFLOW-USG in modeling confined aquifer flow subjected to point source/sink singularity using the standard WEL package. The specification of the well-boundary requires high grid refinement in its vicinity for the generated unstructured grid system. As a result, the overall simulation time of *confinedGWFlowFOAM* for all the solved test examples is significantly higher than the confined groundwater flow model presented in Dey and Dhar (2020). However, the inherent parallel computation strategies of OpenFOAM® overcome this limitation and facilitate the modeling of large-scale aquifer systems by applying *confinedGWFlowFOAM*.

The *wellConfinedBC* boundary condition integrates the effects of finite well radius, well-bore storage, well-bore skin, and partial well penetration to specify the time-varying hydraulic head at the well-boundary for unsteady well-hydraulics problems. However, the proposed well-boundary approach for a partially penetrating well does not estimate the vertical flow occurring in the vicinity of the well. For simulating the vertical flow, the 3D confined groundwater flow equation needs to be utilized as done in *subsurfaceFlowFOAM* (Dey and Dhar 2022), instead of the depth-averaged governing equation. Nevertheless, *confinedGWFlowFOAM* can be successfully applied for estimating the overall drawdown characteristics of large-scale regional confined aquifer systems subjected to pumping through fully or partially pumping wells with considerable accuracy.

Furthermore, *reducedConfinedGWFlowFOAM* replicates the results of *confinedGWFlowFOAM* with desirable accuracy at considerably reduced CPU times, satisfying grid-convergence characteristics. The most computationally expensive steps of reduced-order modeling are the snapshot matrix formation and the subsequent process of pattern identification from it. The process of snapshot generation generally starts with a small Δt value which gradually increases on approaching the final snapshot time T_s . Due to large Δt values, the symmetric Gauss-Seidel solver requires a large number of iterations to converge for a solver tolerance of 10^{-6} m, which at times exceeds the maximum iteration limit of 1000 set as default in OpenFOAM®. Therefore, for the sake of the accuracy of the snapshot matrix, the maximum iteration limit was increased, which eventually increased the CPU time of the offline algorithm. The offline procedure of precomputation involves matrix multiplication and inversion operations. For grid systems with a large number of elements, the dimension of the coefficient matrix \mathbf{A} is high, and the corresponding precomputation procedure involves ample CPU time and memory. However, the CPU usage is always significantly low for the combined offline operations of snapshot matrix formation

Table 5 Comparison of error statistic parameters and CPU computation speedup for *reducedConfinedGWFlowFOAM*

Test case	maxAE (m)	MAE (m)	RMSE (m)	NRMSE	CPU simulation time (s)		CPU speedup
					<i>confinedGW-FlowFOAM</i>	<i>reducedConfinedGW-FlowFOAM</i>	
TC-2	5.50×10^{-3}	2.41×10^{-3}	2.96×10^{-3}	4.77×10^{-4}	80.73	0.17	~470
TC-3	1.47×10^{-2}	8.77×10^{-3}	9.61×10^{-3}	2.40×10^{-3}	162.89	1.34	~121
TC-4	5.27×10^{-2}	6.53×10^{-4}	1.48×10^{-3}	3.90×10^{-4}	6,275.39	8.22	~764
TC-5	1.37×10^{-2}	3.28×10^{-3}	4.06×10^{-3}	1.10×10^{-3}	742.66	0.44	~1697
TC-6	2.70×10^{-2}	9.10×10^{-3}	1.07×10^{-2}	2.68×10^{-3}	348.28	2.11	~165

maxAE maximum absolute error; NRMSE normalized root mean square error

and precomputation compared to the full-system solution applying *confinedGWFlowFOAM*.. Applying *reducedConfinedGWFlowFOAM*, this study has achieved a 470 and 121 times reduction in CPU computation time for the single-well confined aquifer pumping test under homogeneous (TC-2) and heterogeneous (TC-3) conditions. Computation time reduction is much more significant for problems with complex flow mechanisms and Neumann boundary conditions involving a large number of grid elements, which has been evident from TC-4 and TC-5, in that they achieved a 764 and 1,697 times reduction in CPU times, respectively.

Summary and conclusions

This research paper presents an OpenFOAM® library, *modFlowFOAM*, to simulate a variety of confined groundwater flow problems ranging from steady-state hydraulic head distribution to unsteady well hydraulics. The *modFlowFOAM* library includes both the full-system solver, *confinedGWFlowFOAM*, and the reduced-order solver, *reducedConfinedGWFlowFOAM*, alongside the boundary conditions *wellConfinedBC*, *pumpingConfinedBC* and *specifiedConstantConfinedGWFluxBC*, custom-made specifically for confined-aquifer flow problems. Developing *modFlowFOAM* on the open-source platform of OpenFOAM® has been a unique attempt toward generalized confined aquifer flow modeling, enhancing its applicability among practitioners for solving practical problems. The *modFlowFOAM* results for the considered test examples show perfect agreement with the results of MODFLOW and other published works from the literature, which prove the potential applicability of the solvers in estimating well-flow characteristics and groundwater dynamics for regional confined aquifer systems subjected to variable boundary conditions.

Acknowledgements All the simulations were performed utilizing the resources and supercomputing facilities of ‘Param Shakti’ at the Indian Institute of Technology Kharagpur, established under the National Supercomputing Mission (NSM), supported by the Ministry of Electronics and Information Technology (MeitY) and Department of Science and Technology (DST), Government of India, and implemented by the Centre for Development of Advanced Computing (CDAC), Pune.

Funding The authors declare that no funds, grants, or other support were received during the preparation of this paper.

Code availability The source code for *modFlowFOAM* can be downloaded from the link: <https://github.com/gwres/modFlowFOAM>.

Declarations

Competing Interests The authors declare that they have no known competing financial interests or personal relationships that could have appeared to influence the work reported in this paper.

References

- Agarwal RG, Al-Hussainy R, Ramey HJ (1970) An investigation of well-bore storage and skin effect in unsteady liquid flow: I. analytical treatment. *Soc Pet Eng J* 10(03):279–290
- Barenblatt GI, Zheltov IP, Kochina IN (1960) Basic concepts in the theory of seepage of homogeneous liquids in fissured rocks [strata]. *J Appl Math Mech* 24(5):1286–1303
- Barua G, Bora SN (2010) Hydraulics of a partially penetrating well with skin zone in a confined aquifer. *Adv Water Resour* 33(12):1575–1587
- Bear J (1979) *Hydraulics of groundwater*. McGraw-Hill, New York
- Boyce SE, Yeh WW-G (2014) Parameter-independent model reduction of transient groundwater flow models: application to inverse problems. *Adv Water Resour* 69:168–180
- Boyce SE, Nishikawa T, Yeh WW-G (2015) Reduced order modeling of the Newton formulation of MODFLOW to solve unconfined groundwater flow. *Adv Water Resour* 83:250–262
- Cau P, Lecca G, Putti M, Paniconi C (2002) The influence of a confining layer on saltwater intrusion under surface recharge and groundwater extraction conditions. *Dev Water Sci* 47:493–500
- Clifton PM, Neuman SP (1982) Effects of kriging and inverse modeling on conditional simulation of the Avra Valley Aquifer in southern Arizona. *Water Resour Res* 18(4):1215–1234
- Dey S, Dhar A (2020) On proper orthogonal decomposition (POD) based reduced-order modeling of groundwater flow through heterogeneous porous media with point source singularity. *Adv Water Resour* 144(10):103703
- Dey S, Dhar A (2022) Generalized mass-conservative finite volume framework for unified saturated unsaturated subsurface flow. *J Hydrol* 605:127309
- Dougherty DE, Babu DK (1984) Flow to a partially penetrating well in a double-porosity reservoir. *Water Resour Res* 20(8):1116–1122
- Fan Z, Parashar R (2020) Transient flow to a finite-radius well with well-bore storage and skin effect in a poroelastic confined aquifer. *Adv Water Resour* 142:103604
- Haasdonk B, Ohlberger M (2011) Efficient reduced models and a posteriori error estimation for parametrized dynamical systems by offline/online decomposition. *Math Comput Model Dyn Syst* 17(2):145–161
- Hantush MS (1961) Drawdown around a partially penetrating well. *J Hydraul Div* 87(4):83–98
- Hantush MS (1964) Hydraulics of wells. *Adv Hydrosci* 1:281–432
- Harbaugh AW (2005) MODFLOW-2005, The U.S. Geological Survey modular ground-water model: the ground-water flow process. US Geological Survey Techniques Methods 6-A16
- Hasenauer J, Löhning M, Khammash M, Allgöwer F (2012) Dynamical optimization using reduced order models: a method to guarantee performance. *J Process Control* 22(8):1490–1501
- Horgue P, Soulaine C, Franc J, Guibert R, Debenest G (2015) An open-source toolbox for multiphase flow in porous media. *Comput Phys Commun* 187:217–226
- Jasak H, Jemcov A, Tukovic Z, et al. (2007) OpenFOAM: A C++ library for complex physics simulations. In: International Workshop on Coupled Methods in Numerical Dynamics, vol 1000. IUC Dubrovnik Croatia, August 2007, pp 1–20
- Konikow LF, Hornberger GZ, Halford KJ, Hanson RT (2009) Revised multi-node well (MNW2) package for MODFLOW ground-water flow model. US Geol Surv Tech Methods 6-A30
- Liu X (2013) Parallel modeling of three-dimensional variably saturated groundwater flows with unstructured mesh using open source finite volume platform OpenFOAM. *Eng Appl Comput Fluid Mech* 7(2):223–238
- Lohman SW (1972) *Ground-water hydraulics*, vol 708. US Gov Print Off, Washington, DC
- Orgogozo L (2015) RichardsFoam2: a new version of RichardsFoam devoted to the modelling of the vadose zone. *Comput Phys Commun* 196:619–620

- Orgogozo L (2022) RichardsFoam3: a new version of RichardsFoam for continental surfaces hydrogeology modelling. *Comput Phys Commun* 270:108182
- Orgogozo L, Renon N, Soulaine C, Hénon F, Tomer SK, Labat D, Pokrovsky OS, Sekhar M, Ababou R, Quintard M (2014) An open source massively parallel solver for Richards' equation: mechanistic modelling of water fluxes at the watershed scale. *Comput Phys Commun* 185:3358–3371
- Panday S, Langevin CD, Niswonger RG, Ibaraki M, Hughes JD (2013) MODFLOW-USG version 1: An unstructured grid version of MODFLOW for simulating groundwater flow and tightly coupled processes using a control volume finite-difference formulation. *US Geol Surv Tech Methods* 6-A45
- Park HM, Cho DH (1996) Low dimensional modeling of flow reactors. *Int J Heat Mass Trans* 39(16):3311–3323
- Park HM, Chung OY, Lee JH (1999) On the solution of inverse heat transfer problem using the Karhunen-Loeve Galerkin method. *Int J Heat Mass Trans* 42(1):127–142
- Pasetto D, Guadagnini A, Putti M (2011) POD-based Monte Carlo approach for the solution of regional scale groundwater flow driven by randomly distributed recharge. *Adv Water Resour* 34(11):1450–1463
- Pasetto D, Putti M, Yeh WW-G (2013) A reduced-order model for groundwater flow equation with random hydraulic conductivity: application to Monte Carlo methods. *Water Resour Res* 49(6):3215–3228
- Petersen JS, Rohwer C, Albertson ML (1955) Effect of well screens on flow into wells. *Trans Am Soc Civ Eng* 120(1):563–585
- Siade AJ, Putti M, Yeh WW-G (2012) Reduced order parameter estimation using quasilinearization and quadratic programming. *Water Resour Res* 48(6):W06502
- Sirovich L (1987) Turbulence and the dynamics of coherent structures. I. coherent structures. *Q Appl Math* 45(3):561–571
- Stanko ZP, Boyce SE, Yeh WW-G (2016) Nonlinear model reduction of unconfined groundwater flow using POD and DEIM. *Adv Water Resour* 97:130–143
- Stehfest H (1970) Algorithm 368: numerical inversion of Laplace transforms [D5]. *Commun ACM* 13(1):47–49
- Streltsova-Adams TD (1978) Well hydraulics in heterogeneous aquifer formations. *Adv Hydrosci* 11:357–423
- Theis CV (1935) The relation between the lowering of the piezometric surface and the rate and duration of discharge of a well using groundwater storage. *EOS Trans Am Geophys Union* 16(2):519–524
- Tsai FT-C (2006) Enhancing random heterogeneity representation by mixing the kriging method with the zonation structure. *Water Resour Res* 42, W08428
- Ushijima TT, Yeh WW-G (2013) Experimental design for estimating unknown groundwater pumping using genetic algorithm and reduced order model. *Water Resour Res* 49(10):6688–6699
- Vermeulen PTM, Heemink AW, Te Stroet CBM (2004) Lowdimensional modelling of numerical groundwater flow. *Hydrol Process* 18(8):1487–1504
- Wen Z, Zhan H, Wang Q, Liang X, Ma T, Chen C (2017) Well hydraulics in pumping tests with exponentially decayed rates of abstraction in confined aquifers. *J Hydrol* 548:40–45
- Yeh H-D, Chang Y-C (2013) Recent advances in modeling of well hydraulics. *Adv Water Resour* 51:27–51
- Yeh H-D, Chen Y-J, Yang S-Y (2008) Semi-analytical solution for a slug test in partially penetrating wells including the effect of finite-thickness skin. *Hydrol Proc* 22(18):3741–3748
- Zhan H, Park E (2003) Horizontal well hydraulics in leaky aquifers. *J Hydrol* 281(1–2):129–143

Publisher's note Springer Nature remains neutral with regard to jurisdictional claims in published maps and institutional affiliations.

Springer Nature or its licensor (e.g. a society or other partner) holds exclusive rights to this article under a publishing agreement with the author(s) or other rightsholder(s); author self-archiving of the accepted manuscript version of this article is solely governed by the terms of such publishing agreement and applicable law.